Internal Structures of Highlands in Western Lunar Farside Revealed by CE-2 CELMS Data

Zhiguo Meng, *Member, IEEE*, Changbao Yang, Ke Gao, Yongchun Zheng, Zongyu Yue, Yongzhi Wang, Mengna Dong, Jietao Lei, and Shuo Hu

***Abstract*—The internal structures are the key to understand the surface evolution of the Moon. However, the study of such kind is absent. In this study, the Chang'e-2 microwave radiometer data are employed to explore the internal structures in the highlands of the western lunar farside combined with the $FeO+TiO_2$ abundance data and the rock abundance data. The results are as follows. First, a new view on the cratering mechanism is proposed according to the brightness temperature (TB) performances and the estimated rock abundances in King, Bruno, and Necho craters. Second, the influential mechanism of the rocks on the TB is initially identified by the thermal anomalies at noon and night. Third, a special hidden hot anomaly centered at (109.4°E, 6.9°N) northwest to King crater is revealed by the 3.0 GHz map at noon and night but its causes are still unclear. Fourth, the cause of the belt anomaly from Bruno crater to Necho crater has likely resulted from the impact ejecta of King crater. Finally, the highlands in the study area are divided into four units with distinct TB performances. Generally, the TB maps show a different view compared with the optical and thermal infrared data, which is important to improve understanding the surface evolution of the Moon.**

***Index Terms*—CELMS data, internal structures, microwave propagation, thermal anomaly, thermophysical features, western lunar farside.**

Manuscript received February 25, 2020; revised May 12, 2020 and June 17, 2020; accepted August 11, 2020. Date of publication August 18, 2020; date of current version August 31, 2020. This work was supported in part by the National Key R&D Program of China under Grant 2017YFC0602203, in part by the Open Fund of State Key Laboratory of Remote Sensing Science (OFSLRSS201911), in part by the Fundamental Research Funds for the Central Universities, in part by the opening fund of State Key Laboratory of Lunar and Planetary Sciences (Macau University of Science and Technology), Macau FDCT under Grant 119/2017/A3, in part by the Science and Technology Development Fund of Macau under Grant 0012/2018/A1, in part by the National Key Research and Development Project, in part by the Research on Bionic Coupling Dual Bit Self-Balancing Drilling Tool System (2018YFC0808201-4), in part by the Deep-Sea Drilling Technology and Engineering Support (Guangzhou Marine Geological Survey) Project, and in part by the Ultra-Deep Water Coring Drilling Technology and Equipment (Bionic Coring Bit) (DD20190584). *(Corresponding authors: Changbao Yang; Ke Gao.)*

Zhiguo Meng is with the College of Geoexploration Science and Technology, Jilin University, Changchun 130012, China, with the State Key Laboratory of Remote Sensing Science, Aerospace Information Research Institute,Chinese Academy of Sciences, Beijing 100101, China, and also with the State Key Laboratory of Lunar and Planetary Sciences, Macau University of Science and Technology, Macau (e-mail: mengzg@jlu.edu.cn).

Changbao Yang, Yongzhi Wang, Mengna Dong, Jietao Lei, and Shuo Hu are with the College of Geoexploration Science and Technology, Jilin University, Changchun 130012, China (e-mail: yangcb@jlu.edu.cn; wangyongzhi@jlu.edu.cn; dongmn19@mails.jlu.edu.cn; leijt19@mails.jlu.edu.cn; whosure@126.com).

Ke Gao is with the College of Construction Engineering, Jilin University, Changchun 130012, China (e-mail: gaokenm@jlu.edu.cn).

Yongchun Zheng is with the Key Laboratory of Lunar and Deep-space Exploration, National Astronomical Observatories,Chinese Academy of Sciences, Beijing 100864, China (e-mail: zyc@nao.cas.cn).

Zongyu Yue is with the State Key Laboratory of Remote Sensing Science, Aerospace Information Research Institute,Chinese Academy of Sciences, Beijing 100864, China (e-mail: yuezy@radi.ac.cn).

Digital Object Identifier 10.1109/JSTARS.2020.3017204

I. Introduction

When studying the highlands with the Diviner lunar radiometer data, a belt with fairly high nighttime temperature clearly occurs in the western lunar farside, which originates from Giordano Bruno (Bruno) crater (102.9°E, 36.0°N) through King (120.5°E, 5.0°N) and Necho (123.2°E, 5.3°S) craters, and terminates at the Tsiolkovskiy (129.0°E, 20.4°S) crater [1]–[3]. However, no more discussion is proposed for the anomaly. Notably, after studying the geology and stratigraphy of King crater, Heather and Dunkin [4] suggested the presence of a batholithic intrusion, whose southern edge appears to have been within King, and which extends to at least 50 km north of King. Gifford *et al*. [5] also reported the existence of the linear structure along the same direction in Necho crater. Therefore, whether there exists an intrinsic relationship between the thermal anomaly belt and the aforementioned structures, probably internal structures, should be further studied using the data with penetration capabilities.

The pursuit of revealing the internal structures is one of the important goals in the current lunar study [6]–[8]. The internal structures of the Moon are well studied with the gravity data [7]; however, the low-resolution data limit the applications in understanding the shallow layer of the Moon. Moreover, the observations at ultraviolet through the thermal infrared wavelength are also rather limited, for the penetration depth of the signals is no more than 10 s μm [9], [10]. In such depths, the *in situ* regolith is heavily influenced by the space weathering [10], [11].

The spaceborne and *in situ* radar provides another way to probe the internal structures of the shallow layer of the lunar surface [12]–[14]. As the in-orbit lunar radar sounder onboard the Kaguya satellite, it provides a good visualization of the internal features of the Moon in depth more than 1 km [12]. The *in situ* lunar penetration radar in Chang'e (CE)-3/4 missions gives a detailed description of the internal structures from several tens of centimeters to several hundred meters, which is important to improve understanding the evolution of the lunar regolith and even the basaltic volcanism in the landing sites [13], [14]. However, the exploration of the internal structures in the shallow layer, and the study on the relationship between the surface structure indicated by the optical-to-thermal infrared data and

This work is licensed under a Creative Commons Attribution 4.0 License. For more information, see https://creativecommons.org/licenses/by/4.0/

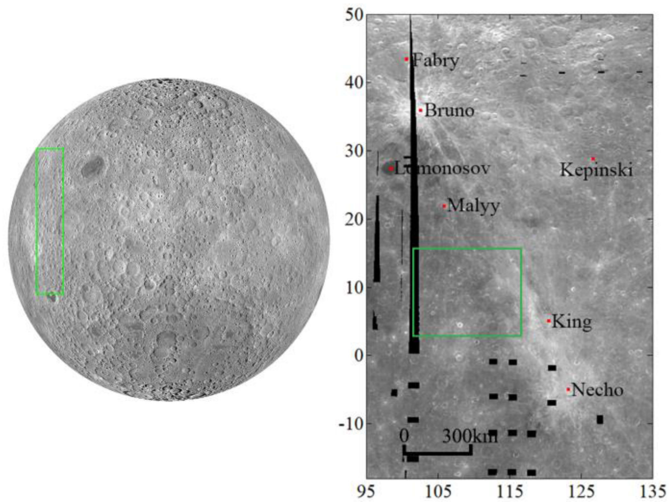

(a) (b)

Fig. 1. (a) Position of the study area (green rectangle) on the lunar farside. (b) Clementine (750 nm) image of the study area, which is downloaded from https://astrogeology.usgs.gov/search/map/Moon/Clementine/UVVIS. The rectangle in green is a special region indicating hot anomaly mentioned in Section III-A3. (The unit used for the geological coordinate system is given in decimal degree. One degree equals about 30 km.).

the deep anomaly revealed by the gravity data are still absent in the global range.

Interestingly, the observations with the passive microwave method provide a new way to evaluate the internal features of the lunar regolith in the shallow layer [15]–[21]. With the microwave radiometer (CELMS) data obtained with the CE-1 satellite, Chan *et al*. [17] and Zheng *et al*. [18] suggested the potential capability of the data in revealing the internal structures of the shallow lunar surface. Meng *et al*. [19]–[21] analyzed the difference of the findings revealed by the CE-2 CELMS data and those by spectral data in several mare regions. Notably, in the global brightness temperature maps provided by Chan *et al*. [17] and Zheng *et al*. [18], [22], the aforementioned belt also exists indicated by the different thermal performances with time and frequencies.

Bruno crater, 22 km in diameter, has been noted as the youngest lunar crater of its size or larger [23]. King crater, 76 km in diameter, and Necho crater, 36 km in diameter, are also young in Copernican age. Moreover, they are located in the highlands of the western lunar farside (see Fig. 1), and the $FeO+TiO_2$ abundance (FTA) in this region is rather low, which means the large penetration depth of the used microwave signal [9], [24]. Thus, this region is considered to be a proper candidate to evaluate the potential capabilities of the CELMS data in understanding the internal structures of the shallow lunar surface [4], [9], [10], [25], [26].

Therefore, in this article, the brightness temperature (TB) measured by the CELMS instrument onboard CE-2 satellite is employed to study the potential internal structures in the highlands of the western lunar farside, including Bruno, King, and Necho craters. Section II briefly introduces the process of the employed data. Section III analyzes the TB features and their applications in studying the internal structures of the shallow lunar surface. Section IV presents the conclusions.

II. Data Processing

The goal of this study is to evaluate the possible applications of the CELMS data in understanding the internal features of the lunar regolith in the shallow layer. Therefore, the radiative transfer simulation is first introduced to evaluate the parameters that can apparently influence the TB of the lunar regolith, which is essential in the following discussions.

A. Radiative Transfer Simulation

A popular two-layer (regolith-rock) model was used [27], [28]. T_B (TB used in this study) measured by the CELMS instrument comprises of the radiation from the regolith layer, T_{B1}, and the radiation from the rock layer, T_{B2}. T_{B1} also includes radiation upwelling, T_{1up}, and downwelling, T_{1dn}. Considering that the observation angle is 0°, the radiative transfer simulation can be expressed as follows:

$$T_B = T_{B1} + T_{B2} = T_{1\mathrm{up}} + T_{1\mathrm{dn}} + T_{2\mathrm{up}}. \tag{1}$$

Here

$$dT_{1\mathrm{up}} = \frac{1-r_1}{1-L} k_{a1}(z)T(z)\mathrm{e}^{-\int_0^z k_{a1}(z')\mathrm{d}z'} dz \tag{2a}$$

$$dT_{1\mathrm{dn}} = \frac{(1-r_1)r_2}{1-L} k_{a1}(z)T(z)\mathrm{e}^{-\left(\int_z^d k_{a1}(z')dz' + \int_0^d k_{a1}(z')dz'\right)} dz \tag{2b}$$

$$dT_{2\mathrm{up}} = \frac{(1-r_1)(1-r_2)}{1-L} k_{a2}(z)T(z)\mathrm{e}^{-\int_\mathrm{d}^z k_{a2}(z')dz'} dz \cdot \mathrm{e}^{-\int_0^d k_{a1}(z')dz'} \tag{2c}$$

where d is the lunar-regolith-layer thickness. k_{a1} and k_{a2} are the absorption coefficients in the lunar regolith and rock layers, respectively. *T(z)* is the temperature profile within the lunar regolith, which is dominated by the surface temperature, the surface slope, and the dielectric constant of the lunar regolith. r_1 and r_2 symbolize the effective reflectivity values of the free space-regolith interface and regolith-rock interface, respectively, which are controlled by the dielectric constants of the lunar regolith, rock, and the surface roughness [29]. $1/(1-L)$ is the multireflection coefficient, which is only related to r_1, r_2, and d.

Therefore, (2) indicates that the measured CELMS data are mainly influenced by such parameters as the dielectric constant $\varepsilon_1(z)$, the surface slope and roughness, and the thickness of the lunar regolith layer.

Among the abovementioned parameters, $\varepsilon_1(z)$ is dominated by the FTA [11], [30], [31]. Moreover, the rock abundance (RA) is always thought as the decisive parameter for the regions with the nighttime hot anomaly in the thermal infrared range [1]–[3] and with the nighttime cold anomaly in the microwave range [17], [18], [20], [22], [26]. Thus, the estimated FTA and RA maps are introduced in this study.

However, the study area is the typical highlands in the lunar farside, and the average thickness of the lunar regolith is more than 10 m [11]. This is much thicker than the penetration depth of the microwave used by the CELMS instrument [20], [32]. Moreover, considering the observation angle of the CELMS instrument is 0°. Thus, the influences of the regolith thickness

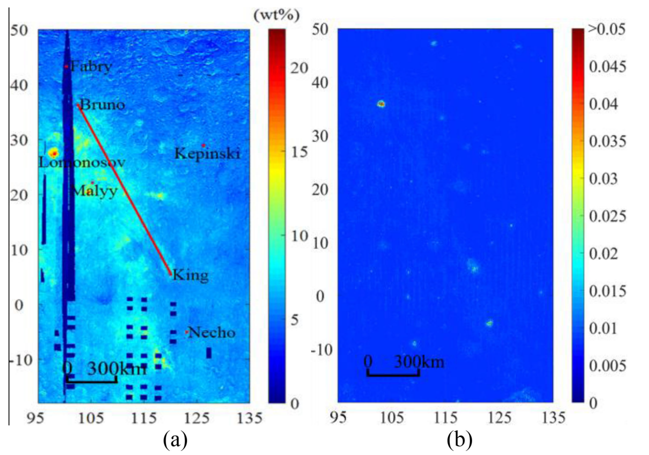

Fig. 2. Distribution of (a) FTA and (b) RA (100%) of the highlands in the western lunar farside. The red line is largely a composition boundary divided the study area into southwestern and northeastern parts. (The unit used for the geological coordinate system is given in decimal degree. One degree equal about 30 km).

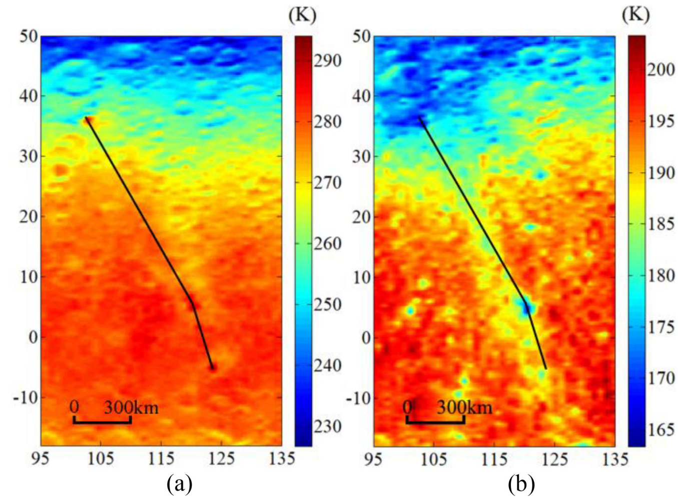

Fig. 3. TB maps of the highlands in the western lunar farside at 37.0 GHz. The black line from Bruno crater to King crater corresponds to the red line in Fig. 2(a) and it can be extended to Necho crater at the night map. (The unit used for the geological coordinate system is given in decimal degree. One degree equals about 30 km.) (a) Noon. (b) Night.

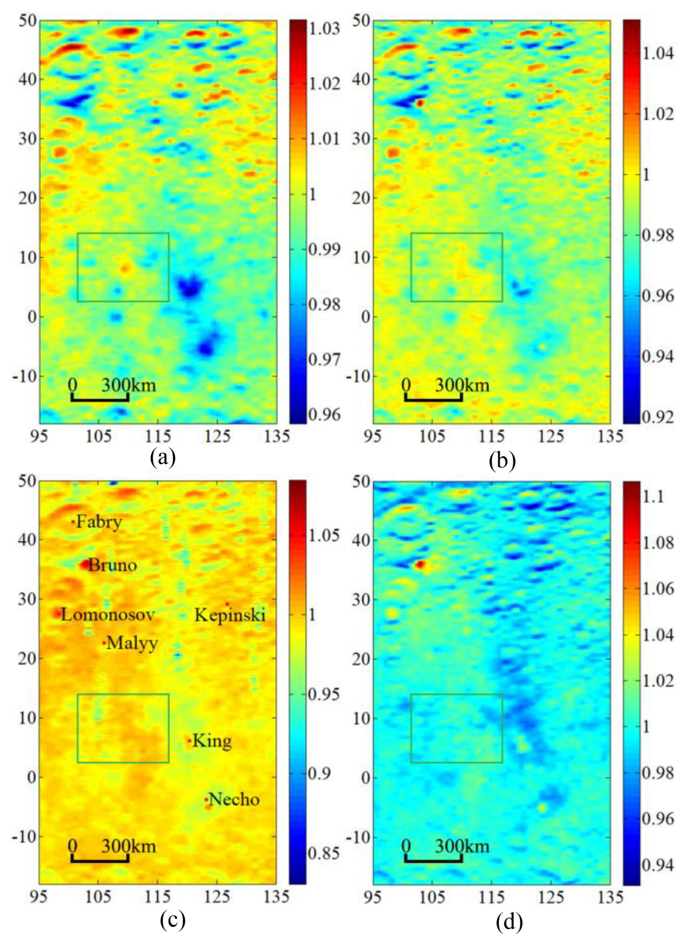

Fig. 4. nTB map of the highlands in the western lunar farside at noon. The rectangle in green is a special region indicating hot anomaly mentioned in Section III-A3. (The unit used for the geological coordinate system is given in decimal degree. One degree equals about 30 km.) (a) 3.0 GHz. (b) 7.8 GHz. (c) 19.35 GHz. (d) 37.0 GHz.

d and surface roughness on the TB are neglected in this study according to the simulation results with (1).

Because the surface slope may alter the effective solar illumination, the evaluation of the TB and nTB (normalized TB generated in the following section) performances should take the surface slope into account. However, Meng *et al*. [20], [21], [26] suggested that the CELMS data are weakly affected by the surface topography according to the comparison between the TB-related map and the topography in Hertzsprung Basin, Apollo Basin, and Mare Moscoviense. Thus, the surface topography is neglected in the extensive regions of the study area, while the topography is considered in the TB-related performances in typical craters due to the large variations of the surface temperature caused by slopes.

B. FTA Map

The FTA is first estimated with the Clementine ultraviolet-visible (UV/VIS) data first. The Clementine mission returned global imaging data collected by the UV/VIS camera. The method developed by Lucey *et al*. [33] is widely used to retrieve the FTA [see Fig. 2(a)], which is also used in this study. The UV/VIS data was downloaded from the USGS network[1].

Fig. 2(a) indicates that the FTA in abundant regions is rather low, less than 10 wt.%. Several phenomena should be mentioned. First, if a line [red line in Fig. 2(a)] is drawn from Bruno crater to King crater, the FTA in the southwest part is higher than that in the eastern part. Second, the region with a relatively higher FTA largely extends from Bruno crater to Necho crater in a belt shape. Third, the FTA in Lomonosov crater (98.3°E, 27.4°N) and the region around Malyy crater (105.6°E, 22.0°N) is the highest in the study area. Considering the shallow penetration depth of the UV-VIS data, the comparison between the FTA performances in Fig. 2(a) and TB performances in Figs. 3 –6 implies the space weathering effect in the study area.

[1]Online. [Available]: http://webgis.wr.usgs.gov/pigwad/down/moon_dl.htm

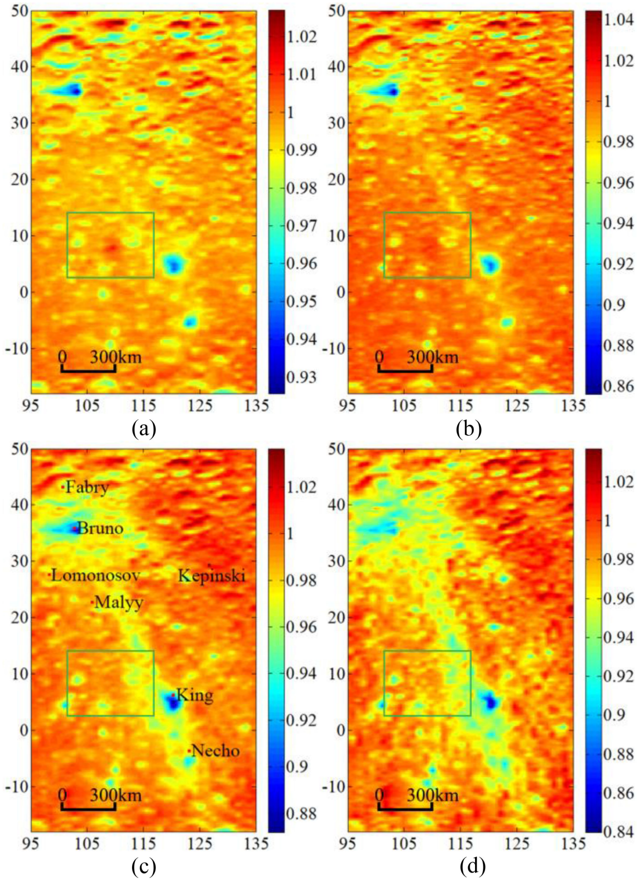

Fig. 5. nTB map of the highlands in the western lunar farside at night. The rectangle in green is a special region indicating hot anomaly mentioned in Section III-A3. (The unit used for the geological coordinate system is given in decimal degree. One degree equals about 30 km.) (a) 3.0 GHz. (b) 7.8 GHz. (c) 19.35 GHz. (d) 37.0 GHz.

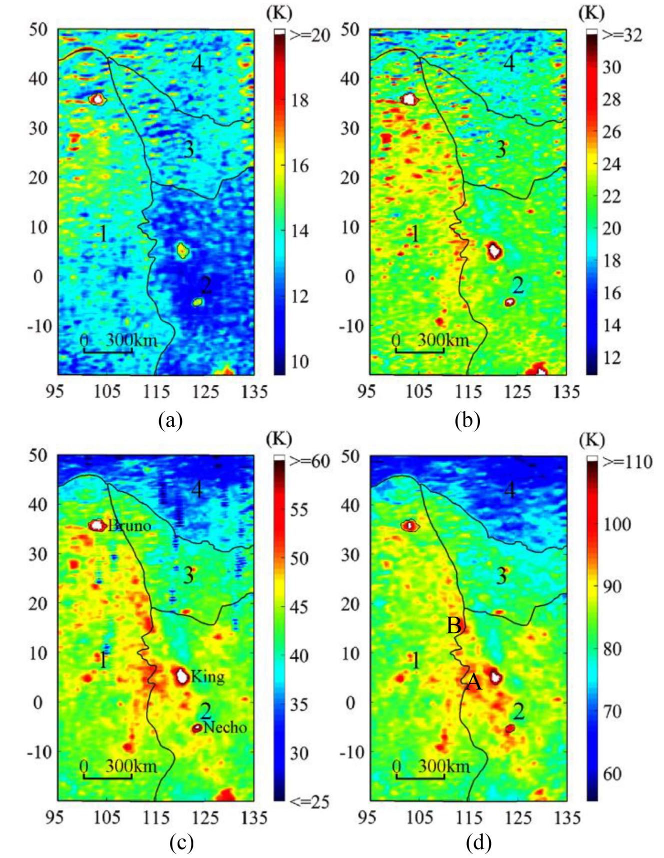

Fig. 6. dTB map of the highlands in the western lunar farside. The black lines surrounding Bruno, King, and Necho craters indicate the range that generates the average dTB values in Table I. The black lines divided the study area into four regions that are mentioned in Section III-C. (The unit used for the geological coordinate system is given in decimal degree. One degree equals about 30 km.) (a) 3.0 GHz. (b) 7.8 GHz. (c) 19.35 GHz. (d) 37.0 GHz.

C. RA Map

Data recorded by the Diviner instrument onboard the LRO satellite were used to estimate the RA in the study area with the method developed by Bandfield *et al*. [1] [see Fig. 2(b)]. The Diviner instrument was operated in the thermal infrared range, which is identified as strongly correlates with the RA of the lunar surface [1]. The Diviner data were downloaded from[2].

Fig. 2(b) shows that the RA in the study is rather low, less than 0.01 in extensive regions. Only in Bruno, King, and Necho craters, the RA is considerably high. The highest RA occurs in Bruno crater, which is more than 0.05, followed by Necho crater, and the RA in King is the lowest among the three craters. The comparison between the RA and the following four-channel TB may present a distinctive understanding of the cratering mechanism of the Moon.

D. TB-Related Maps

CE-2 satellite was the second Chinese lunar orbiter launched on October 1, 2010. One of the main payloads is the microwave radiometer (CELMS) instrument. The CELMS instrument operated at 3.0, 7.8, 19.35, and 37 GHz. The integration time is set as 200 ms [10], [34]. The observation angle is 0° and the temperature sensitivity is better than 0.5 K. The 2C-level data were generated after the system calibration and geometric correction. The data are available on request from[3]. A detailed description of the CELMS instrument and data were given by Cai and Lan [10], Meng *et al*. [20] and [21], and Zhu *et al*. [34]. The same data processing method is adopted in this study.

At first, the hour angle is introduced to attribute the CELMS data to 24 h, which can eliminate the influence of the observation time or surface temperature on the TB maps [19], [35]. For the limited number of the original CELMS data, only the TB from 6 to 7 o'clock and from 13 to 14 o'clock is enough to cover the whole study area. The numbers of the selected CELMS data are 27 834 from 13 to 14 o'clock and 28 143 from 6 to 7 o'clock, which can represent the TB at noon and nighttime, respectively. Then, a linear interpolation method was used to generate the TB maps at 3.0, 7.8, 19.35, and 37.0 GHz with a spatial resolution of $0.25° \times 0.25°$ (see Fig. 3).

[2]Online. [Available]: http://pds-geosciences.wustl.edu/

[3]Online. [Available]: http://moon.bao.ac.cn/searchOrder_pdsData.search

In Fig. 3, the belt with fairly high nighttime temperature mentioned by the Diviner studies [1]–[3] from Bruno crater to Necho crater also clearly presents in the microwave TB maps, which indicate high values at noon but a colder behavior at night. However, the change of the TB with the latitude is great, up to 70 K at noon and more than 40 K at night. Such TB variation is much larger than the TB variation in the aforementioned belt, which is no more than 5 K higher at noon and lower at night than the beyond regions. This is an adverse effect on understanding the regolith thermophysical features in the belt. To eliminate this effect, the nTB proposed by Meng *et al.* [19]–[21] is also introduced. First, one TB is selected for every integer degree of latitude, where the surface parameters mainly including FTA and RA should be similar in the local regions. Thereafter, a fitting curve was constructed for the selected TB at every channel, and the fitted value was defined as the standard TB of the corresponding latitude. Finally, eight fitting curves are constructed as the standard TB at noon and night, and the nTB is calculated through dividing the generated TB by the fitted standard TB along the corresponding latitude [see Figs. 4 and 5].

Compared with Fig. 3, the influence of the surface temperature with the latitude is significantly weakened. This is particularly obvious in the nTB maps at night. Therefore, Figs. 4 and 5 are proper to evaluate the internal features of the lunar regolith in the corresponding penetration depth of the used microwave.

Moreover, the dTB, defined as the difference between the daytime TB and the night TB of the same frequency, is also proposed to be directly related to the regolith thermophysical parameters within the penetration depth of the corresponding microwave [19], [20], [31]. Therefore, the dTB maps were also generated with the noon TB and night TB obtained above (see Fig. 6). Compared with Figs. 3–5, Fig. 6 indicates a new view of Bruno, King, Necho craters, and the deposits in the shallow surface.

For the CELMS, the first orbital instrument to measure the microwave thermal emission of the lunar regolith [22], it is hard to evaluate the rationality of the generated TB-related maps. Apparently, the low night nTB values are just located in Bruno, King, and Necho craters, where fairly high dTB values exist as well. This indicates the rationality of the TB-related maps in geographical positions. Moreover, the TB maps of the whole Moon were available in works by Chan *et al.* [17] and Zheng *et al.* [18] using CE-1 CELMS data and the works by Cai and Lan [10] and Zheng *et al.* [22] using CE-2 CELMS data. Our TB maps agree with their results in values and the daytime-nighttime performances, in particular, the belt anomaly from Bruno crater to Necho crater. Therefore, our TB-related maps are rational.

However, two issues should be mentioned.

First, the noon nTB is high in the north inner wall and low in the south inner wall of Fabry crater (100.7°E, 43.1°N), which shows that the surface slope plays a significant role on the generated nTB maps. Nevertheless, the study area is mainly within the low-latitude region, which can weaken the impact of the surface slope to some extent. Moreover, the high noon nTB in the north inner wall and low noon nTB in the south inner wall of Fabry crater are not apparent in the dTB maps, validating that the surface slope plays a weak role in the dTB maps. Thus, the dTB maps are essential in evaluating the internal structures of the study area.

Second, there occur several belts with abnormally low nTB values in Fig. 4(c), indicating the problem of the data quality of the CELMS data in this channel and the following Fig. 6(c). Despite this setback, the TB beyond the anomaly belts presents a good correlation with the nTB and dTB performances in the other three channels. Therefore, the 19.35 GHz nTB and dTB maps are only used as a reference in this study.

Additionally, for the absence of the water in the lunar regolith and the low FTA in the study area, the signal in the microwave range can penetrate the regolith up to 20× the wavelength [19], [35], that is, the penetration depth is up to 2 m at 3.0 GHz, 77 cm at 7.8 GHz, 31 cm at 19.35 GHz, and 16.2 cm at 37 GHz. Therefore, Figs. 4–6 are able to disclose the internal features of the lunar regolith in this extensive region.

III. Results and Discussions

Figs. 4–6 reveal some interesting information about the regolith and the ejecta compared with the optical results.

A. Thermal Anomalies

The cold and hot thermal anomalies are fundamentally important to understand the thermal performances of the lunar regolith. Figs. 2, 4–6 show some meaningful clues about the cold and hot anomalies, and the typical craters.

1) New View About the Cratering Mechanism: There exist abundant cold anomalies with relatively lower nTB than their vicinities in Fig. 5, which are most apparently located in Bruno, King, and Necho craters. The causes for the cold anomalies are widely accepted as the high RA. Hu *et al.* [36] and Liu and Jin [37] verified the findings with the numerical simulation using the radiative transfer equation. Meng *et al.* [26] also validated the finding with the TB performances in the typical craters with high RA surrounding the Hertzsprung basin. Again, the positive coincidence between the nTB and dTB performances and the high RA values in Bruno, King, and Necho craters validates that the RA is the cause for the night cold anomalies and the high dTB anomalies in Figs. 5 and 6.

The similar nTB and dTB performances indicate the similarity of the regolith thermophysical parameters in the cold anomalies. Thus, a new view of the cratering mechanism can be hypothesized according to the nTB and dTB performances in Bruno, King, and Necho craters, as the nTB maps at night and dTB maps show a good distribution of the regolith thermophysical parameters with depth.

At 3.0 and 7.8 GHz, the lowest nTB is in Bruno crater, the value of which is as similarly low as King crater at 19.35 GHz, and the lowest nTB occurs in King crater at 37 GHz. The dTB maps illustrate the thermal performances more clearly, as is presented in Table I. At 3.0 GHz, the average dTB in Bruno crater is about 3 K higher than that in King crater, it is only 2 K higher than the latter at 7.8 GHz, while the average dTB in King crater is much higher than that in Bruno crater at 19.35 and 37 GHz. The dTB in Necho crater is always the lowest.

TABLE I
AVERAGE DTB (K) IN BRUNO, KING, AND NECHO CRATERS

	3.0 GHz	7.8 GHz	19.35 GHz	37.0 GHz
Bruno	18.1	34.6	59.5	98.0
King	15.3	32.6	62.4	107.6
Necho	14.9	30.5	56.4	97.4

Therefore, combined with the relationship between the RA and the TB, the nTB and dTB performances likely indicate that the RA is the highest in Bruno crater in the deep layer revealed by the 3.0 and 7.8 GHz maps, corresponding to the depth larger than 31 cm until greater than 2 m. But in the upward direction from the depth 31 cm represented by the 19.35 GHz microwave, the RA in King crater is apparently higher than that in Bruno crater. Comparatively, the RA in Necho crater is the lowest in the CELMS microwave penetration range but it is much higher than the nearby highlands. That is, the four-channel TB maps give a good description of the RA changes of the three mentioned craters in the vertical direction.

The previous studies presented that the diameters of Bruno, Necho, and King are 22, 37, and 76 km, and the corresponding ages are 1–10 Ma, 80 Ma, and 1 Ga, respectively [4], [5], [23]. Thus, the probable RA distribution with the depth gives a hypothesis about the evolution of the large boulders in the craters.

The large crater (e.g., King crater) excavated more large boulders from the shallow crust. Even after hundreds of millions of years of space weathering, the RA is still fairly high in the shallow layer but it is a bit low in the deep layer.

The small crater (e.g., Bruno crater) excavated fewer large boulders compared with the large craters. The crater in such sizes, then, indicates a small region with a rather high RA but the space weathering quickly shuttles the large boulders in the shallow layer, and the large boulders in the deep layer are kept. If the time for space weathering is long enough, the large boulders in the deep layer become undetectable as in Necho crater.

Notably, the RA map obtained from the Diviner thermal infrared data shows much higher values in Bruno and Necho craters. Considering the penetration abilities of the thermal infrared signal, the RA in the surface layer revealed by the Diviner data is probably different from that in the deep layer revealed by the microwave data.

This is the first time we evaluated the RA distribution in the vertical direction. Although there also exists many other factors that can influence the propagation of the microwave, the generally homogenous FTA in Fig. 2(a) and surface topography make us confident that it is the change of RA that brought the difference in nTB and dTB performances with frequencies.

Moreover, Figs. 4–6 also present that there exist many more craters with similarly apparent low night nTB and high dTB anomaly, some of which are not indicated by the RA map as those at the region near (123°E, 19°N). Furthermore, there are many more ancient craters with no TB and RA anomalies.

Therefore, the nTB performances, or more likely the dTB performances, post a new understanding of the relationship between the RA distribution and the ages and sizes of the craters, which is helpful to improve the understanding of the cratering mechanism of the Moon. The strong correlation between the RA and the dTB values may provide a new way to evaluate the age of the typical craters, deserved to be further studied with more sources of data.

2) New View About RA Influence on Temperature Profile: The influence of RA on the thermal emission is always a highlighted topic over the lunar surface. Here, the high nighttime TB in the thermal infrared domain is undoubtedly attributed to the existence of the rocks, which is revealed by the Diviner data [1]–[3]. However, in the microwave range, the influence is still in debate. Chan *et al*. [17] and Zheng *et al*. [18] found that the cold anomalies at night are highly related to the hot anomalies indicated by Bandfield *et al*. [1], and they proposed that the high RA values will bring about the hot TB anomaly at noon and cold anomaly at night over the lunar surface. Hu *et al*. [36] and Liu and Jin [37] verified the conclusion with the radiative transfer simulation and the thermal conduction model.

The nTB performances in Fig. 5 verify the existence of low TB in the regions with high RA values at night. However, the noontime nTB performances in Fig. 4 give a different view on the change of the temperature with depth. In Fig. 4, the nTB in the regions with high RA values is low at 3.0 GHz, while it becomes fairly high at 19.35 and 37 GHz.

That is, at noon, the regions with high RA values will have a comparatively lower physical temperature in the depth indicated by the 3.0 GHz microwave, while they become relatively warmer in the shallow layer from the depth indicated by the 7.8 GHz microwave. At night, the regions with high RA values have a fairly cold temperature in depth revealed by the four-channel CELMS data, while they are warmer in the surface layer indicated by the Diviner data.

For the first time, we proposed that the regions with higher RA values below the superficial layer indicate a cold temperature in the deep layer both at noon and at night, which postulates a new view about the temperature distribution in the regions with high RA values. No reports have been done to interpret the special temperature profile brought by the high RA values until now.

3) A Special Hot Anomaly: Different from the Diviner work, the CELMS hot anomaly at night is more likely related to the volcanic features in mare regions [19], [21].

Figs. 4 and 5 indicate a special hot anomaly located at the spot near (109.4°E, 6.9°N) (green rectangle in Figs. 1, 4, and 5). At noon, the nTB in this spot is clearly higher than its vicinity at 3.0 GHz, while it becomes similar to the vicinity in the other three channels. At night, the nTB here is nearly the highest in the south part at 3.0 GHz; it is a bit higher than the nearby regions at 7.8 GHz, and the anomaly is again absent at the other two channels. Combined with the penetration abilities of the used microwave, this indicates that the hot anomaly should be a hidden construct.

Then, what is the cause of the hot anomaly? Fig. 2 indicates that the FTA and RA values in this spot are similar to its vicinity. Fig. 7 is the WAC image of the spot, referred to as the green rectangle in Figs. 1(b), 4, and 5, where a green dashed ellipse is drawn surrounded by six large craters. However, there are no

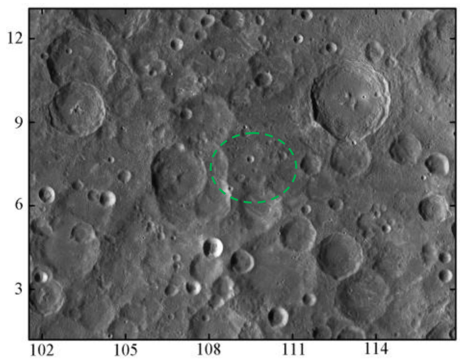

Fig. 7. Mosaic of WAC image of the hot anomaly. (The unit used for the geological coordinate system is given in decimal degree. One degree equals about 30 km).

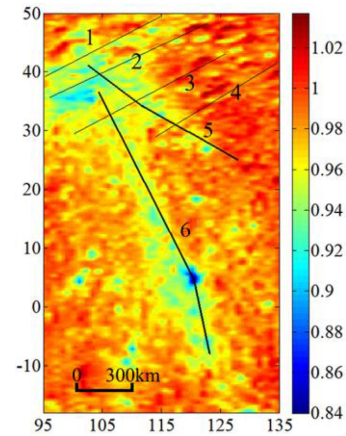

Fig. 8. Linear structure revealed by the nTB map (37.0 GHz, night). (The unit used for the geological coordinate system is given in decimal degree. One degree equals about 30 km).

topographic features responsible for the nTB anomaly. That is, the FTA, RA, and the surface slope can be excluded from the causes for the hot anomaly. Moreover, the dTB performances are not abnormal in this spot. Similar dTB values indicate the similar thermophysical parameters of the lunar regolith within the penetration depth, verifying that this is a hidden construct with a hot anomaly.

Interestingly, a similar hot anomaly was also found in Maria Moscoviense and Orientale, which are proposed as the elevated physical temperature in the substrate [21], [28]. However, different from the previous finding, this spot is in the highlands, and the elevated substrate temperature is not appropriate to interpret the hot anomaly as the volcanic activity is absent here.

The hidden hot spot is about 50×50 km in size, indicating that it is a relatively strong temperature-related activity. This is the first time we found the hot anomaly in the highland regions. The pursuit of the formation mechanism of the anomaly will provide some interesting information about the thermal evolution of the Moon. This spot deserves to be further studied.

B. *Internal Structures of the Belt Anomaly*

When studying the highlands with the Diviner data, a belt with fairly high nighttime temperature clearly occurs in the western lunar farside, which originates from Bruno crater through King and Necho craters and terminates at Tsiolkovskiy crater [1]–[3]. In the global TB maps provided by Chan *et al*. [17] and Zheng *et al*. [18] and [22], this belt still exhibits low values at night. However, no more discussion is proposed for the anomaly.

The nTB and dTB maps in Figs. 4–6 indicate a different view about the belt, as presented in Fig. 8, which is expressed as follows.

1) The belt is not clear at daytime nTB maps. At 3.0 and 7.8 GHz maps, there occur two regions with the cold anomaly surrounding King and Necho craters, which is elongated in the north–northwest direction. The regional anomalies become faint at 19.35 and 37 GHz maps. This hints that the daytime nTB maps are not proper to evaluate the belt anomaly.
2) The belt anomaly is clearly presented with relatively lower nTB at the nighttime maps, although the belt is not clear at 3.0 GHz. At 7.8 GHz, there exists a clear line between Bruno and King craters with a width of about 30 km. At 19.35 and 37 GHz, the belt anomaly is clearly presented from the north of Bruno crater through King crater and terminated at the south of Necho crater, and the width of the belt is about 160 km at 19.35 GHz and more than 300 km at 37 GHz. The length of the belt is more than 1200 km, indicating that the belt anomaly is considerably large in size.
3) The dTB maps also show that the belt is not visible at the 3.0 GHz map. The belt is still not clear at 7.8 GHz but a boundary seems to occur from Bruno crater to King crater, as mentioned in Fig. 2(a), which divides the highlands into the relatively lower dTB in the northeastern part and the relatively higher dTB in the southwestern part. Also, multiple places with relatively higher dTB exist along the belt. At 19.35 GHz, the belt can be easily seen and it is even more clearly expressed at the 37 GHz map.

Thus, the belt anomaly should have resulted from the special deposits in the shallow layer, existing in depth larger than 77 cm (penetration depth of 7.8 GHz microwave) but lower than 2 m (penetration depth of 3.0 GHz microwave). Moreover, the width of the belt is small at the depth indicated by the nTB and dTB performances from 7.8 to 37 GHz, which agrees with the change of the surface materials by the impact ejecta using the numerical simulation of the cratering mechanism [38]. That is, the belt anomaly is the original highland materials altered by the impact ejecta. This then prompts the question, “The ejecta of which crater should be responsible for the belt?”

Gifford *et al*. [5] and Basilevsky and Head [39] suggested that the belt in the optical data is the ejecta ray from Bruno crater. This is because it is the youngest in age, it is quite large in size, and the ejecta rays will extend a large distance as that in Tycho crater. Moreover, the ejecta rays from Bruno crater are also found in Mare Smythii with a continuously special albedo compared with the background highlands, which has a similar distance as the belt anomaly [39]. Combined with the thermal anomaly in Diviner map, it seems that the belt anomaly should be attributed to the ejecta from Bruno crater.

TABLE II
POSITION, LENGTH (L), WIDTH (W), AND PROBABLE DEPTH (D) OF THE INTERNAL LINEAR STRUCTURES

No.	Start	End	L (km)	W (km)	D(cm)
1	95.0°E, 38.9°N	114.7°E, 49.4°N	530	91	>31
2	96.0°E, 35.2°N	122.7°E, 48.2°N	719	104	>31
3	100.2°E, 28.9°N	125.8°E, 43.0°N	756	95	>200
4	114.0°E, 28.4°N	134.6°E, 41.3°N	643	106	>200
5	100.7°E, 43.1°N	126.7°E, 28.6°N	824	120	>200
6	104.3°E, 36.3°N	123.2°E, 9.7°S	1520	300	> 77

However, the nTB and dTB performances do not support the conclusion for the following three reasons.

1) The distribution of the cold nTB and high dTB anomaly in the northern part surrounding Bruno crater is generally in the northeast direction, which is different from the beyond region in the north–northwest direction. The difference in the anomaly direction indicates a different view of the distribution of the ejecta deposits from Bruno crater.
2) The ejecta from Bruno crater also reaches Mare Smythii in another direction but it is not indicated by the CELMS data as that performed in the belt anomaly.
3) At 37 GHz, the nTB is low at night, and the dTB is high in the west of King crater [Marked *A* in Fig. 6(d)], which is similar to the nTB and dTB performances in the region marked *B* along the belt in Fig. 6(d). The similarity in the nTB and dTB performances indicates the homogeneity in regolith thermophysical features.

Therefore, the belt anomaly has likely resulted from the impact ejecta of King crater, not the Bruno crater. Interestingly, the width of the belt anomaly is the largest near King crater, validating the rightness of our conclusion.

After studying the geologic features of King crater, Heather and Dunkin [4] proposed the presence of a batholithic intrusion, whose southern edge appears to have been within King and extends to at least 50 km north of King. The agreement between the belt anomaly and the batholithic intrusion indicates a new view of the formation mechanism of King crater and, even, the highlands in the western lunar farside, which should be paid more attention in future studies.

Besides the aforementioned belt anomaly, there exists a linear structure or belt from Fabry crater (100.7°E, 43.1°N) to Kepinski crater (126.7°E, 28.6°N), which is clearly indicated by the low nTB at night. The belt anomaly is also exhibited at 3.0 GHz, indicating that the depth of the structure is more than 2 m. Moreover, the linear structure is also the boundary of the highlands between the relatively higher dTB in the northeastern part and the southwestern part.

Additionally, there exist another four linear structures in the northeast direction marked 1–4 in Fig. 8 and the related parameters are presented in Table II. Lines 1 and 2 are shown as a boundary between the low and high nTB values at 19.35 and 37 GHz, and Line 3 is indicated by multiple spots with cold anomalies at 3.0 and 7.8 GHz at night, whereas Line 4 is a structure with relatively higher nTB values at the four channels at night.

The internal belt and linear structures indicate a new understanding of the surface evolution in the ancient lunar highlands. More work should be done to better understand these internal structures.

C. Internal Regolith Features

Compared with the nTB maps at noon and night that experience a strong influence from the surface slope, the four-channel dTB maps indicate a good description of the regolith thermophysical parameters in the corresponding penetration depth.

As shown in Fig. 6, the regolith thermophysical parameters change greatly from the deep layer indicated by the 3.0 GHz map to that revealed by the 37 GHz map. At 3.0 GHz, the dTB in the southeastern part is rather low, about 10 to 13 K, while it is about 14 to 17 K in the northeastern and western part. At 7.8 GHz, the difference between the southeastern part and the northeastern part becomes not clear but the difference between the eastern part and the western part is enhanced, where the boundary of the two parts follows the line mentioned in Figs. 2(a) and 3, and the distribution of the belt anomaly. At 19.37 and 37 GHz, the difference between the eastern part and the western part becomes even more apparent, while the average dTB in the southeastern part is higher than that in the northeastern part. Meanwhile, there exists a region with the lowest dTB in the north part.

Therefore, the highland regions can be divided into four units, as shown in Fig. 6. Unit 1 is in the western part, which always indicates a relatively higher dTB. Unit 2 is in the southeastern part, which indicates a low dTB at 3.0 GHz but the second-highest dTB at the other three channels. Unit 3 is in the northeastern part, which indicates a second-highest dTB at 3.0 GHz but a second-lowest dTB at 19.35 and 37 GHz. The northern part is attributed to Unit 4, which indicates the lowest dTB at 19.35 and 37 GHz.

This surface division is very different from the optical image and even the FTA map. Here, the optical image in Fig. 1 indicates a relatively darker tone in the western part compared with the eastern part. This means that the regolith in the western part is a bit rich in mafic deposits, which agrees with the FTA distribution in Fig. 2(a). This also gives a good interpretation of the higher dTB in Unit 1, which agrees with the relatively higher dTB values according to the theoretical simulation [9], [21].

Moreover, dTB performances in Unit 4 hint that there exists a special deposit with a thin layer, the depth of which is larger than 31 cm but less than 77 cm. The continuous and irregular distribution of the Unit hints the existence of the special material but it could not identify the material only by the CELMS data.

In Unit 2, the lowest dTB at 3.0 GHz and the second-highest dTB at 19.35 and 37 GHz hint the great change of the regolith thermophysical parameters with depth. The change of the regolith parameters with depth is also great in Unit 3 according to the dTB performances in different channels.

Again, it is impossible to identify what materials brought about the internal regolith structures of such kind. More work and sources of data, including the high-spatial-resolution geophysical data and *in situ* observations, should be employed to further explore the internal regolith features in this highland region.

IV. Conclusion

In this study, the TB, nTB, and dTB maps generated with the CE-2 CELMS data are employed to analyze the internal features of the lunar regolith in the western part of the lunar farside. Combined with the FTA map and the penetration capabilities of the microwave, several interesting results can be obtained.

First, a new view of the cratering mechanism is hypothesized according to the nTB and dTB performances in King, Bruno, and Necho craters. The RA in the large crater (e.g., King crater) is still fairly high in the shallow layer but it is a bit low in the deep layer. The small crater (e.g., Bruno crater) indicates a small region with a rather high RA, while the large boulders in the deep layer are abundantly distributed.

Second, a new view of the RA influence on the temperature profile is proposed according to the nTB performances at noon and night. At noon, the regions with high RA values will have a comparatively lower physical temperature in the deep layer indicated by the 3.0 GHz microwave, while they become relatively warmer in the shallow layer from the depth indicated by the 7.8 GHz microwave. At night, the regions with high RA values will be fairly cold in temperature in depth revealed by the four-channel CELMS data but it is warm in the surface layer indicated by the Diviner data.

Third, a special, hidden hot anomaly is revealed by the 3.0 GHz map at noon and night but its causes are still in doubt. This is the first time that we found such kind of hot spot in highland places, which is not related to topography or FTA anomalies.

Fourth, the belt anomaly from Bruno crater to Necho crater indicated by the nTB at night is thoroughly analyzed with the dTB maps. The result indicates that the belt anomaly is likely due to King crater. Additionally, at least five more linear structures are proposed by the nTB performances at night.

Finally, the highlands in the study area are divided into four units according to the dTB performances at the four channels, which shows the change of the regolith thermophysical features with depth.

Generally, the nTB and dTB maps show a different view compared with the optical data. The findings of the hidden hot anomaly, the linear structures, and the division of the highlands are of great significance to improve understanding the surface evolution of the Moon. This deserves to be further studied with more sources of the data in the future.

Acknowledgment

The authors would like to thank the people helping with this work. In this study, the WAC data were downloaded from http://wms.lroc.asu.edu/lroc/search, the UV/VIS data were downloaded from http://webgis.wr.usgs.gov/pigwad/down/moon_dl.htm, and the Diviner data were downloaded from http://pds-geosciences.wustl.edu/.

References

[1] J. L. Bandfield, R. R. Ghent, A. R. Vasavada, D. A. Paige, S. J. Lawrence, and M. S. Robinson, "Lunar surface rock abundance and regolith fines temperatures derived from LRO diviner radiometer data," *J. Geophys. Res. Planets*, vol. 116, no. E12, 2011, Art. no. E00H02.

[2] P. Hayne *et al.*, "Global regolith thermophysical properties of the moon from the diviner lunar radiometer experiment," *J. Geophys. Res. Planet.*, vol. 122, pp. 2371–2400, 2017.

[3] J. P. Williams, D.A. Paige, B.T. Greenhagen, and E. Sefton-Nash, "The global surface temperatures of the moon as measured by the diviner lunar radiometer experiment," *Icarus*, vol. 283, pp. 300–325, 2017.

[4] D. J. Heather and S. K. Dunkin, "Geology and stratigraphy of King crater, lunar far-side," *Icarus*, vol. 163, no. 2, pp. 307–329, 2003.

[5] A. W. Gifford, T. A. Maxwell, and F. El-Elbaz, "Geology of the lunar farside crater necho," *Moon Planets*, vol. 21, no. 1, pp. 25–42, 1979.

[6] H. Hiesinger, J. Head, U. Wolf, G. Neukum, and R. Jaumann, "Ages of mare basalts on the lunar nearside: A synthesis," *J. Geophys. Res. Planet.*, vol. 105, pp. 29239–29275, 2000.

[7] N. Namiki *et al.*, "Farside gravity field of the moon from four-way Doppler measurements of SELENE (Kaguya)," *Science*, vol. 323, pp. 900–905, 2009.

[8] C. Chisenga, J. Yan, J. Zhao, E. A. Atekwana, and R. Steffen, "Density structure of the Rümker region in the northern oceanus procellarum: Implications for lunar volcanism and landing site selection for the Chang'E-5 mission," *J. Geophys. Res. Planet.*, vol. 125, no. 1, 2020, Art. no. e2019JE005978.

[9] T. Fang and W. Fa, "High frequency thermal emission from the lunar surface and near surface temperature of the Moon from Chang'E-2 microwave radiometer," *Icarus*, vol. 232, pp. 34–53, 2014.

[10] Z. Cai and T. Lan, "Lunar brightness temperature model based on the microwave radiometer data of Chang'e-2," *IEEE Trans. Geosci. Remote Sens.*, vol. 55, no. 10, pp. 5944–5955, Oct. 2017.

[11] B. M. French, D. Vaniman, G. Heiken, *Lunar Sourcebook: A User's Guide to the Moon*. Cambridge, U.K.: Cambridge Univ. Press, 1991.

[12] T. Kobayashi, J. H. Kim, S. R. Lee, H. Araki, and T. Ono, "Simultaneous observation of lunar radar sounder and laser altimeter of Kaguya for lunar regolith layer thickness estimate," *IEEE Trans. Geosci. Remote Sens. Lett.*, vol. 7, no. 3, pp. 435–439, Jul. 2010.

[13] L. Xiao *et al.*, "A young multilayered terrane of the northern Mare Imbrium revealed by Chang'e-3 mission," *Science*, vol. 347, no. 6227, pp. 1226–1229, 2015.

[14] J. L. Lai *et al.*, "Comparison of dielectric properties and structure of lunar regolith at Chang'E-3 and Chang'E-4 landing sites revealed by ground-penetrating radar," *Geophys. Res. Lett.*, vol. 46, no. 22, pp. 12783–12793, 2019.

[15] L. Chappaz *et al.*, "Evidence of large empty lava tubes on the moon using GRAIL gravity," *Geophys. Res. Lett.*, vol. 44, no. 1, pp. 105–112, 2017.

[16] J. S. Jiang and Y. Q. Jin, *Selected Paper on Microwave Exploration of Lunar Surface in Chinese Chang'E-1 Project*. Beijing, China: Science Press, 2011.

[17] K. L. Chan, K. T. Tsang, Bruce Kong, and Yong-Chun Zheng, "Lunar regolith thermal behavior revealed by Chang'E-1 microwave brightness temperature data," *Earth Planet. Sci. Lett.*, vol. 295, no. 1/2, pp. 287–291, 2010.

[18] Y. C. Zheng, K. T. Tsang, K. L. Chan, Y. L. Zou, F. Zhang, and Z. Y. Ouyang, "First microwave map of the Moon with Chang'E-1 data: The role of local time in global imaging," *Icarus*, vol. 219, no. 1, pp. 194–210, 2012.

[19] Z. Meng, S. Hu, T. Wang, C. Li, Z. Cai, and J. Ping, "Passive microwave probing mare basalts in mare imbrium using CE-2 CELMS data," *IEEE J. Sel. Topics Appl. Earth Observ. Remote Sens.*, vol. 11, no. 9, pp. 3097–3104, Sep. 2018.

[20] Z. G. Meng *et al.*, "Thermophysical features of shallow lunar crust demonstrated by typical copernican craters using CE-2 CELMS data," *IEEE J. Sel. Topics Appl. Earth Observ. Remote Sens.*, vol. 12, no. 7, pp. 2565–2574, Jul. 2019.

[21] Z. G. Meng *et al.*, "Reevaluating mare moscoviense and its vicinity using Chang'e-2 microwave sounder data," *Remote Sens*., vol. 12, no. 3, p. 535, 2020.

[22] Y.-C. Zheng *et al.*, "Analysis of *Chang'E-2* brightness temperature data and production of high spatial resolution microwave maps of the Moon," *Icarus*, vol. 319, pp. 627–644, 2019.

[23] T. Morota *et al.*, "Formation age of the lunar crater Giordano Bruno," *Meteoritics Planet. Sci.*, vol. 44, no. 8, pp. 1115–1120, 2009.

[24] B. A. Campbell, L. M. Carter, B. R. Hawke, D. B. Campbell, and R. R. Ghent, "Volcanic and impact deposits of the moon's aristarchus plateau: A new view from earth-based radar images," *Geology*, vol. 36, pp. 135–138, 2008.

[25] K. A. Howard, "Ejecta blankets of large craters exemplified by King Crater, in: Apollo 16 preliminary science report," NASA, Washington, DC, USA, NASA SP-315, 1972.

[26] Z. Meng, Q. Wang, H. Wang, T. Wang, and Z. Cai, "Potential geologic significances of hertzsprung basin revealed by CE-2 CELMS data," *IEEE J. Sel. Topics Appl. Earth Observ. Remote Sens.*, vol. 11, no. 10, pp. 3713–3720, Oct. 2018.

[27] Z. Z. Wang, Y. Li, J. Jiang, and D. Li, "Lunar surface dielectric constant, regolith thickness, and 3He abundance distributions retrieved from the microwave brightness temperatures of CE-1 lunar microwave sounder," *Sci. Chin. Earth Sci.*, vol. 53, no. 9, pp. 1365–1378, 2010.

[28] Z. G. Meng, J. Zhang, Z. Cai, J. Ping, and Z.-S. Tang, "Microwave thermal emission features of Mare Orientale revealed by CELMS data," *IEEE J. Sel. Topics Appl. Earth Observ. Remote Sens.*, vol. 10, no. 6, pp. 2991–2998, Jun. 2017.

[29] F. T. Ulaby, R. K. Moore, and A. D. Fung, *Microwave Remote Sensing: Microwave Remote Sensing Fundamentals and Radiometry*. Reading, MA, USA: Addison-Wesley, 1981.

[30] Y. G. Shkuratov and N. V. Bondarenko, "Regolith layer thickness mapping of the moon by radar and optical data," *Icarus*, vol. 149, no. 2, pp. 329–338, 2001.

[31] Z. G. Meng, G. Yang, J. Ping, Z. Cai, A. Gusev, and E. M. Osei, "Influence of ($FeO+TiO_2$) abundance on the microwave thermal emissions of lunar regolith," *Sci. Chin. Earth Sci.*, vol. 59, no. 7, pp. 1498–1507, 2016.

[32] X. Y. Li, S. Wanga, Y. Zheng, and A. Cheng, "Estimation of solar illumination on the Moon: A theoretical model," *Planet. Space Sci.*, vol. 56, pp. 947–950, 2008.

[33] P. G. Lucey, D. T. Blewett, and B. L. Jolliff, "Lunar iron and titanium abundance algorithms based on final processing of Clementine ultraviolet-visible images," *J. Geophys. Res. Planet.*, vol. 105, no. E8, pp. 20297–20305, 2000.

[34] Y. C. Zhu, Y. Zheng, S. Fang, Y. Zou, and S. Pearson, "Analysis of the brightness temperature features of the lunar surface using 37 GHz channel data from the Chang'e-2 microwave radiometer," *Adv. Space Res.*, vol. 63, no. 1, pp. 750–765, 2019.

[35] Z. Meng, R. Zhao, Z. Cai, J. Ping, Z. Tang, and Si Chen, "Microwave thermal emission at Tycho area and its geological significance," *IEEE J. Sel. Topics Appl. Earth Observ. Remote Sens.*, vol. 10, no. 6, pp. 7616–7619, Jun. 2017.

[36] G.-P. Hu, K. L. Chan, Y.-C. Zheng, and A.-A. Xu, "A rock model for the cold and hot spots in the Chang'E microwave brightness temperature map," *IEEE Trans. Geosci. Remote Sens.*, vol. 56, no. 9, pp. 5471–5480, Sep. 2018.

[37] N. Liu and Y.-Q. Jin, "A radiative transfer model for MW cold and IR hot spots of Chang'e and diviner observations," *IEEE Trans. Geosci. Remote Sens.*, vol. 57, no. 10, pp. 8184–8190, Oct. 2019.

[38] Z. Yue *et al.*, "Projectile remnants in central peaks of lunar impact craters," *Nature Geosci.*, vol. 6, pp. 435–437, 2013.

[39] A. T. Basilevsky and J. W. Head, "Age of Giordano Bruno crater as deduced from the morphology of its secondaries at the Luna 24 landing site," *Planet. Space Sci.*, vol. 73, no. 1, pp. 302–309, 2012.

Zhiguo Meng (Member, IEEE) received the Ph.D. degree in geophysics from Jilin University, Changchun, China, in 2008.

He is currently a Professor with the College of Geoexploration Science and Technology, Jilin University, Changchun. His research interests include the application and development of microwave remote sensing technology in the planetary science, primarily, the microwave measurement of the lunar regolith.

Changbao Yang received the Ph.D. degree in applied geophysics from Jilin University, Changchun, China, in 2004.

He is currently an Associate Professor with the College of Geoexploration Science and Technology, Jilin University, Changchun. His research interests include the application and development of remote sensing technology in the geology and mineral identification.

Ke Gao received the Ph.D. degree in geological engineering from Jilin University, Changchun, China, in 2006.

He is currently a Professor with the College of Construction Engineering, Jilin University. He has authored and coauthored more than 40 scientific papers and 80 patents. His research interests include bionic drilling machines and tools, deep continental scientific drilling, and extraterrestrial star drilling.

Yongchun Zheng received the Ph.D. degree in geochemistry from the University of Chinese Academy of Sciences, Beijing, China, in 2005.

He is currently a Researcher with the National Astronomical Observatories, Chinese Academy of Sciences, Beijing, China. His research interests include the study of lunar and planetary geology, the understanding of the Moon and Mars regolith, the utilization of planetary resources, the surface environment of the planet, the scientific goals and future development strategies of the Moon, and deep space exploration.

Zongyu Yue received the Ph.D. degree in geology from the China University of Geosciences (Beijing), Beijing, China, in 2008.

He is currently a Professor with the State Key Laboratory of Remote Sensing Science, Aerospace Information Research Institute, Chinese Academy of Sciences, Beijing, China. His research interests include the lunar and planetary remote sensing geology, primarily focusing on the impact craters. He has authored or coauthored more than 50 scientific papers.

Yongzhi Wang received the Ph.D. degree in geoexploration and information technology from Jilin University, Changchun, China, in 2008.

From 2015 to 2016, he was a Visiting Scholar with York University. He is currently a Professor with the College of Geoexploration Science and Technology, Jilin University, Changchun. He has authored and coauthored more than 50 scientific papers. His research interests include remote sensing, geoscience big data, and artificial intelligence.

Dr. Wang is a member of the International Association for Mathematical Geosciences.

Mengna Dong is currently working toward the master's degree in geodetection and information technology with the College of Geoexploration Science and Technology, Jilin University, Changchun, China.

Her research interest focuses on the application of microwave remote sensing technology in mineral characteristics.

Jietao Lei is currently working toward the master's degree in cartography and geography information system with the College of Geoexploration Science and Technology, Jilin University, Changchun, China.

His research interests include the application of microwave remote sensing technology in the planetary science and land surface parameters inversion using microwave remote sensing technology.

Shuo Hu is currently working toward the master's degree in cartography and geography information system with the College of Geoexploration Science and Technology, Jilin University, Changchun, China.

His research interests include the application of microwave remote sensing technology in the planetary science and land surface parameters inversion using remote sensing technology.